Plasma Phys. Control. Fusion **40** (1998) A87–A103. Printed in the UK PII: S0741-3335(98)92966-9

ICRF results in D–T plasmas in JET and TFTR and implications for ITER

The JET and TFTR Teams, presented by D F H Start
JET Joint Undertaking, Abingdon, Oxon, UK

Received 23 January 1998

Abstract. Recent experiments in D–T plasmas on the JET and TFTR tokamaks have evaluated a wide range of ITER relevant ion cyclotron heating scenarios. Absorption of fast waves at the second-harmonic tritium resonance has provided bulk ion heating in TFTR supershots and electron heating in JET H-mode discharges. In JET, deuterium minority heating has generated 1.7 MW of fusion power with 6 MW of radio frequency power giving a record steady-state Q-value of 0.22. Strong bulk ion heating has been achieved with He^3 minority heating with central ion temperatures up to 13 keV being produced in H-modes with a density of 3.6×10^{19} m^{-3}. Hydrogen, deuterium and He^3 minority heating methods have produced plasmas with normalized confinement times greater than or equal to that required by ITER for ignition. These H-modes are characterized by small-amplitude, high-frequency ELMs, each of which transports less than 1.5% of the plasma energy content to the limiters. The heavy minority scheme of tritium in a deuterium plasma has been demonstrated both as a heating scheme and a generator of suprathermal neutrons. On TFTR mode conversion to an ion Bernstein wave has achieved central bulk ion heating in supershots with target ion temperatures greater than 20 keV.

1. Introduction

Extensive experimental campaigns have been completed recently on both the JET and TFTR tokamaks. A substantial part of these programmes was devoted to assessing the physics and performance of ion cyclotron resonance heating (ICRH) scenarios in plasmas with up to 95% tritium fraction. The main emphasis was placed on schemes that are directly relevant to the ITER experimental reactor [1]. These comprised minority ion heating with hydrogen, deuterium and He^3 isotopes as well as tritium second-harmonic ICRH. In addition, new results were obtained on innovative methods such as tritium minority heating on JET and mode conversion ion heating on TFTR [2]. This paper reviews the most important results with special emphasis on the implications for ITER. The TFTR experiments reported here were made mainly with combined ICRH and neutral beam injection (NBI) in circular supershot plasmas with high central ion temperatures [3–9]. The JET results were obtained with ICRH alone in single-null, H-mode divertor plasmas with ITER-like shape and safety factor as shown in figure 1. These experiments have produced a record steady-state fusion Q-value of 0.22 with radiofrequency (RF) heating alone [10] and have established ICRH as the unique system for heating the core plasma ions on the route to ignition in a tokamak reactor. The ICRH system on JET consists of four antennas approximately equally spaced around the tokamak. Each antenna has four current straps and any phasing required by the experiments can be applied between these currents. The experiments described in this paper used $0\pi0\pi$ phasing. The RF plant can couple up to 22 MW to the plasma and has

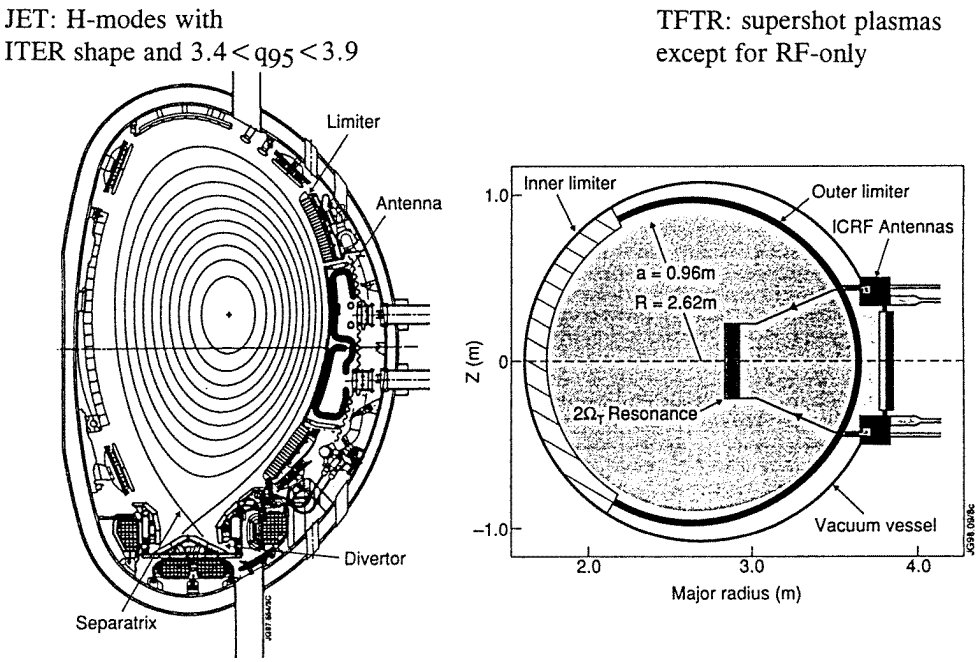

Figure 1. Poloidal cross sections of JET and TFTR showing the different plasma configurations used in the present experiment.

a frequency range of 23–56 MHz to allow a wide range of heating scenarios to be used [11]. The TFTR ICRH system consisted of four two-strap antennas until 1997 and could operate at 43 MHz and 64 MHz at power levels of 11 MW and 6 MW, respectively. In 1997, two antennas were replaced by four-strap modules for mode conversion experiments at 30 MHz [2].

Both JET and TFTR have performed experiments to assess the second-harmonic heating scheme and the results of these studies are presented in the next section. In section 3 the minority heating experiments, mainly investigated at JET, are discussed. The mode conversion experiments in which the ion Bernstein wave (IBW) is observed to give ion heating, as well as electron heating, on TFTR comprise section 4.

2. Heating at the second-harmonic tritium resonance

The best performance of ICRH at the $2\omega_{CT}$ cyclotron resonance in TFTR supershots [3, 4, 5, 7] is shown in figure 2. The toroidal field was 4.2 T which, together with an RF frequency of 43 MHz, placed the $2\omega_{CT}$ resonance in the plasma centre. ICRH power of 5.5 MW was added to 23.5 MW of NBI and gave a central ion temperature, T_{i0}, of 36 keV compared to 26 keV in a similar discharge heated only by beams and with the same NBI power (see also figure 3). The average density was 4×10^{19} m^{-3}. Some electron heating by the RF was also observed and the central electron temperature reached 10.5 keV compared with 8 keV in the comparison pulse. The NBI comprised 60% tritium beam power and the tritium density at the centre of the plasma was about 30% due to a strong deuterium influx from the walls. The discharge contained 2% He^3 in order to improve the coupling to

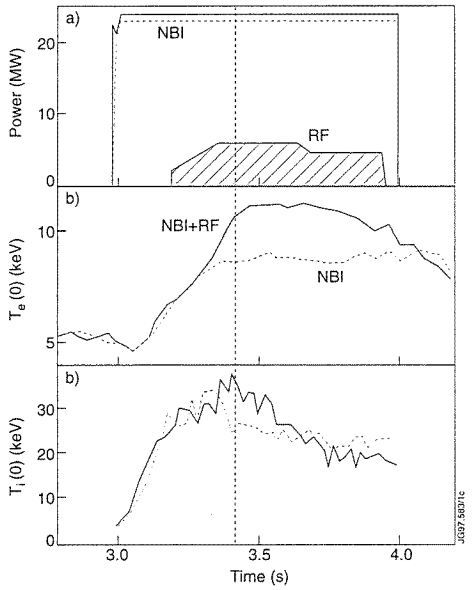

Figure 2. Central ion heating with $2\omega_{CT}$ ICRH in a TFTR supershot. Comparison with a discharge heated by neutral beams alone shows a 10 keV increase in T_{i0} due to the RF.

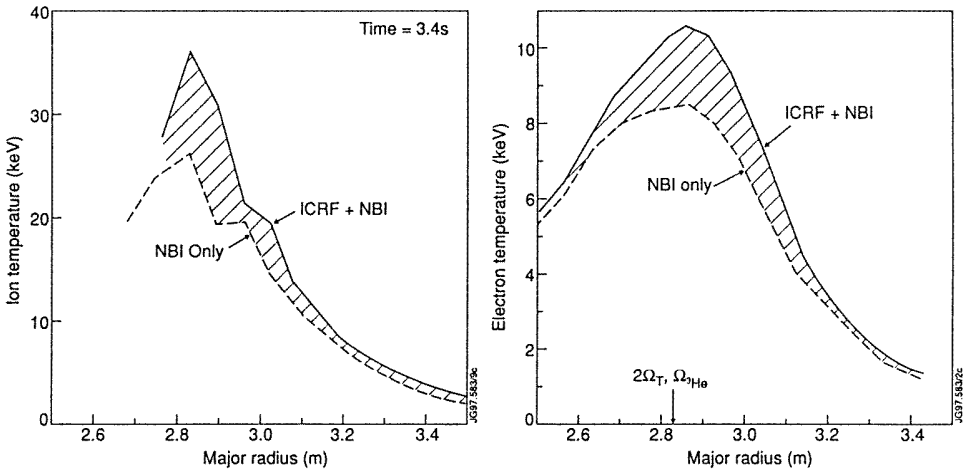

Figure 3. Ion and electron temperature profiles at 3.4 s for the supershots shown in figure 2 with both NBI and NBI + ICRH.

the fast wave by eliminating eigenmodes. Although the He^3 and second-harmonic tritium resonances coincide, the heating was mainly due to absorption by the tritons since a similar discharge without He^3 gave $T_{i0} = 34$ keV with 4.4 MW of ICRH. In addition, no strong ion heating was found in deuterium supershots with He^3 minority heating [4].

The ion and electron heating rates were determined using modulation of the RF power and measurements of the ion and electron temperatures responses [3, 5]. Typical results with no He^3 minority are given in figure 4 and show that the power is deposited centrally

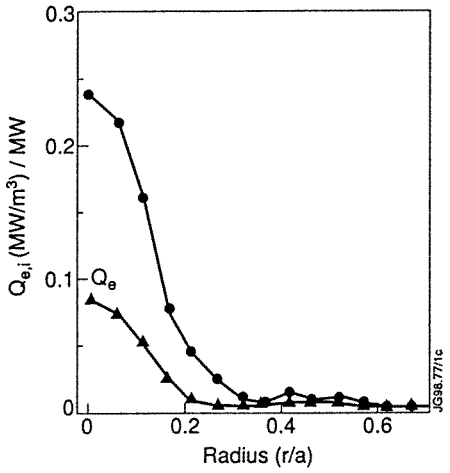

	PISCES	TRANSP	Exp.
Direct Electron Heating	26%	24%	26±10%
Direct ion Heating	43%	59%	59±10%
Mode Conversion	~22%	<10%	5%

JG98.77/1c

Figure 4. ICRH heating profiles determined by modulation techniques and comparison of total heating rates with theoretical calculations.

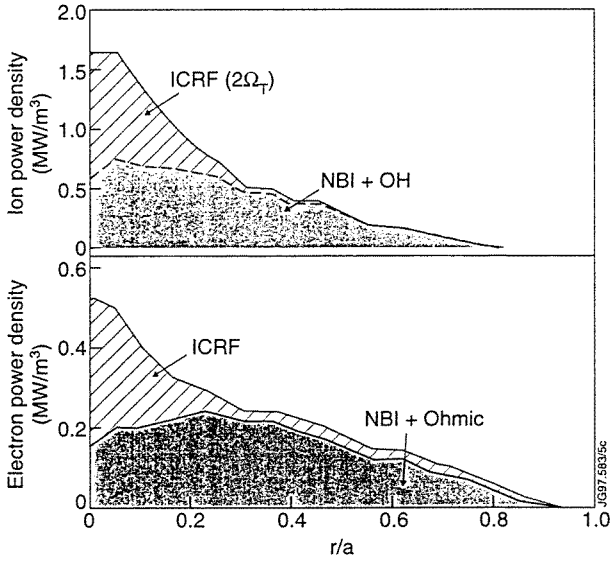

Figure 5. TRANSP calculations showing the twofold increase in the central ion and electron heating power densities due to the ICRH in the discharge shown in figure 4.

and that the fraction flowing to the ions is more than twice that to the electrons. These results agree broadly with the predictions of the TRANSP and PISCES codes as shown in figure 4.

The ion and electron power densities calculated [5] by the TRANSP code are shown in figure 5. The addition of 4.4 MW of ICRH to 23 MW of NBI more than doubles the power densities on-axis for both ions and electrons with the former being increased by 1 MW m^{-3}. Experiments were also made with increasing NBI power which reduced the direct electron heating as expected [3, 4, 7].

Further confirmation that the power was absorbed by $2\omega_{CT}$ ICRH is the observation of fast tritons of at least 600 keV reaching loss detectors in synchronism with modulation of the RF power [3–5]. The effective temperature of the tail of the triton distribution was measured in RF-only heated limiter discharges as shown in figure 6. As the power level is raised the tail temperature shows a modest increase but the fast ion density increases substantially due to influx of particles from the limiter. Also shown in figure 6 are results from the JET fast neutral particle analyser [12] which show a similar triton tail energy.

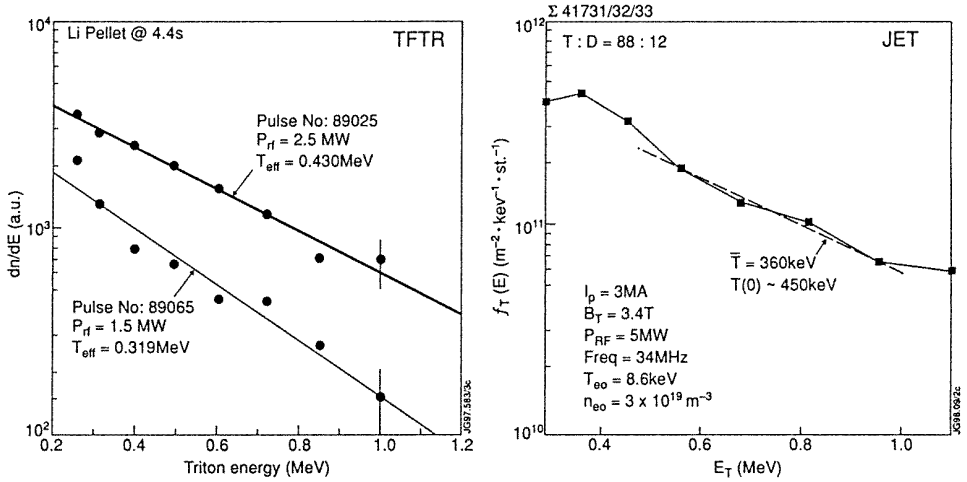

Figure 6. Fast tritons observed in TFTR and JET ICRF-only discharges. In the JET case the distribution function is a summation of three discharges.

The best performance achieved with $2\omega_{CT}$ in JET is shown in figure 7 for an RF power of 8 MW and a D:T ratio of 40:60. The discharge was run with a central density, $n_{e0} = 3.2 \times 10^{19}$ m^{-3} and with a plasma current, $I_p = 3.3$ MA. An H-mode is formed at $t = 14.7$ s as revealed by the appearance of ELMs on the $D_\alpha + T_\alpha$ trace. The plasma stored energy was 5 MJ of which 1 MJ is due to a fast ion component which is produced by the RF acceleration of tritons to high energy. The confinement time for the thermal component, when normalized to the recent ITER H97-P scaling law for ELMy H-modes [13], gives an enhancement factor, H97 = 0.7. This value is less than those achieved with minority heating, $0.85 <$ H97 < 0.95, partly due to the loss of tritons with energy above 4 MeV (corresponding to a 20% power loss [14]), and partly because of the broadening of the heating profile due to the large orbits of these fast tritons. The central electron and ion temperatures reached 8.9 keV and 5.8 keV, respectively, showing the predominance of electron heating as expected with such a strong tail energy. The neutron emission reached 2.5×10^{16} s^{-1} which is mainly due to thermal D–T reactions. The predominance of electron heating has a dramatic effect on the neutron rate which is a factor of six less than that achieved with He^3 minority heating where the ion temperature reached 13 keV (see section 3.1) under similar conditions [10, 15]. Additional evidence for strong tail formation in the $2\omega_{CT}$ discharges is the detection of toroidal Alfvén eigenmodes (TAE modes) excited by resonance with the precessional motion of the fast ion trapped banana orbits [16]. No such eigenmodes are excited in either the D or He^3 minority heating schemes, both of which had tail temperatures of less than 300 keV. The neutron rates observed with $2\omega_{CT}$ heating are well described by calculations using the PION code [17] which includes the

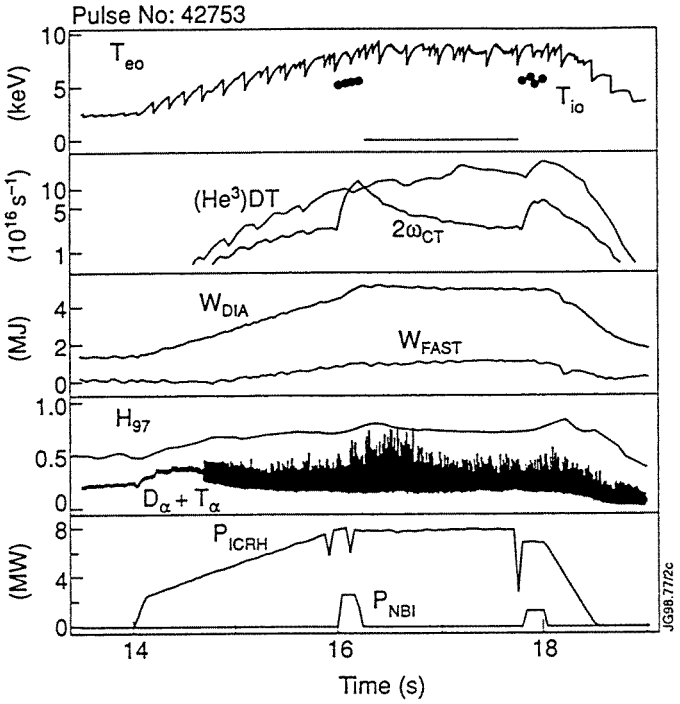

Figure 7. Plasma parameters for 8 MW of $2\omega_{CT}$ ICRH in JET. The neutron yield is 15% compared with He^3 minority heating which produces stronger bulk ion heating.

power absorption and fast ion distribution in a self-consistent way. The neutron production is typically 30% from tail–plasma interactions and 70% thermal in origin. The calculations [14] suggest that 20% of the power is lost through unconfined tritons of energy greater than 5 MeV for 3.3 MA discharges and $n_{e0} = 3.2 \times 10^{19}$ m^{-3}. In addition the calculated power partition is 10:1 in favour of the electrons. However, note that $2\omega_{CT}$ power densities as low as 300 kW m^{-3}, compared with $\sim$1 MW m^{-3} in JET, can be achieved in ITER with 50 MW of RF power which results in mainly ion heating.

Such high tail energies need not arise in ITER and the second-harmonic tritium ICRH scheme will be able to heat ions and electrons equally as shown by the PION calculations in figure 8. These results are for an input power of 50 MW and a D:T ratio of 30:70. The curves shown in figure 8 are contours of constant ion heating fraction in the plane of central density (n_{e0}) and electron temperature (T_{e0}). The dashed line shows the direct route to ignition, $n_{e0} = 1 \times 10^{20}$ m^{-3}, $T_{e0} = 35$ keV [18], from the ohmic target with $n_{e0} = 3.4 \times 10^{19}$ m^{-3} and $T_{e0} = 5$ keV. Along this route the ion heating fraction is close to 70%. To achieve this value the power density to the tritons is kept below 300 kW m^{-3} by means of two resonances to broaden the power deposition as shown in figure 9. Note from the insert that the direct electron damping rises strongly with the value of the parallel wavevector, $k_\parallel$. In the calculations $k_\parallel = 3.1$ which gives an electron damping fraction of 10% for the parameters shown.

In summary, the experiments on TFTR and JET have demonstrated efficient heating and have generated H-modes in divertor plasmas. The TFTR results, with power densities close to 1 MW m^{-3}, have shown that a hot ion target plasma is necessary for ion heating. A similar

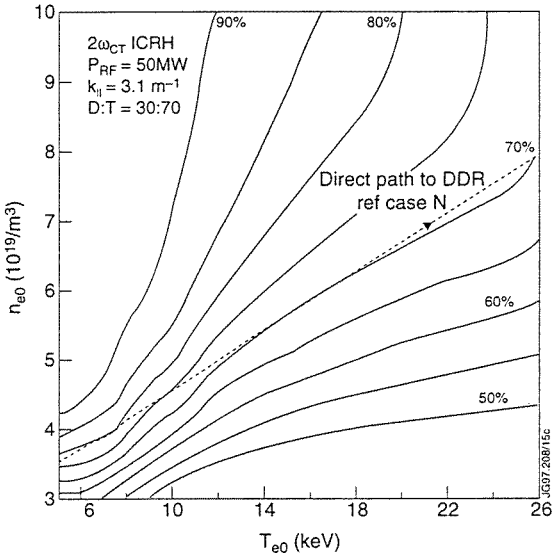

Figure 8. PION calculations for 50 MW of $2\omega_{CT}$ ICRH in ITER. The results are shown as contours of constant ion heating fraction on the n_{e0}, T_{e0} plane.

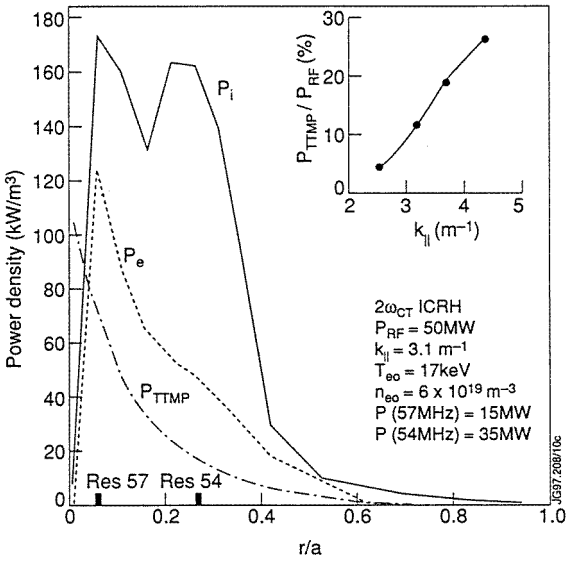

Figure 9. Heating profiles for the ITER ICRH case in figure 8. Two RF frequencies are used to broaden the heating profile. The inset shows the sensitivity of direct electron damping to $k_{\|}$.

effect is seen in JET optimized shear discharges [19] with second-harmonic deuterium ICRH. Otherwise, as in the JET RF-only experiments, electron heating dominates. In present machines there is some loss of the fast tritons, and when this effect is taken into account the heating and neutron rates are well predicted by theory. In ITER the power density can be kept sufficiently low to produce 70% bulk ion heating on the route to ignition without fast ion losses.

3. ICRH with minority ions

3.1. Deuterium and He^3 minority heating

The results for the (D)T and (He^3)DT minority experiments in $I_p = 3.7$ MA, $B_T = 3.7$ T discharges are presented in [10] and also at this meeting [15], and will only be summarized briefly in this paper. The principal achievements are shown in table 1. The (D)T ICRH scenario, with D:T = 9:91, produced 1.7 MW of fusion power for 6 MW of RF power by accelerating the deuterons to the peak of the D–T fusion cross section ($E_d \sim 100$ keV). The discharge reached steady state with a Q-value $= E_{fus}/(E_{RF} + E_{OH}) = 0.22$ for three energy confinement times ($\tau_E \sim 0.8$ s), the pulse length being limited by neutron economy. The central electron temperature was 7.2 keV so that the critical energy [20] was 100 keV, the same as the deuteron energy. As a consequence, the deuterons slowed down equally on electrons and ions giving rise to almost equal ion and electron temperatures. Such bulk ion heating will be a strong asset in achieving ignition on ITER. Evidence for a deuteron energy close to 100 keV was provided by both neutron spectroscopy and the distribution function measured by the fast neutral particle analyser. This instrument detects deuterons in the range 200 keV to 1 MeV and recorded a tail temperature of about 90 keV. Equality of power flow to electrons and ions was also the case with 6.5% He^3 minority heating. With this scenario the neutron production was entirely due to thermal reactions giving 0.5 MW of fusion power for a total power input (RF + ohmic heating) of 10 MW. The normalized confinement times in each case exceeded the ITER ignition requirement (H97 = 0.86). A further requirement for ITER is a limit of 1% [21] on the energy carried to the limiter by each edge-localized mode (ELM). In the JET experiments the ELMs were high frequency and low amplitude. An upper limit on the energy per ELM can be set by assuming that all the energy flowing from the core is exhausted by the ELMs. In this case $\Delta W_{ELM}/W = \tau_{ELM}/\tau_E$, where τ_{ELM} and τ_E are the ELM period and plasma energy confinement time, respectively. Typical values are $\tau_{ELM} = 40$ ms and $\tau_E = 0.8$ s, for the (D)T case giving $\Delta W_{ELM}/W < 0.5\%$. The ELMs are less frequent in the He^3 case where the upper limit exceeds the ITER value.

Table 1. Summary of the principal results of (D)T and (He^3)DT minority ICRH in JET.

Scenario	P_{fusion} (MW)	$Q_{st,state}$	T_{i0}, T_{e0}	P_i/P_e (PION)	$\langle E\rangle/E_{crit}$	H97[a]	$\Delta W_{ELM}/W$
D(T)	1.7 (Supra-therm)	0.22 (0.5 in ITER)	6.6, 7.2	0.8	1.2 ± 0.25 (Exp)	0.90	$< 0.5\%$
(He^3)D–T	0.5 (Thermal)	0.05	13, 11	0.9–1.2	~ 1 (PION)	0.95	$< 1.5\%$

[a] H97 $(\tau/\tau_{ITER\,H-97Py}) = 0.86$ gives ignition on ITER.

Calculations for ITER for the He^3 scheme give similar results to those for the $2\omega_{CT}$ scheme as shown in figure 10. This figure shows a case with $P_{RF} = 50$ MW and a He^3 fraction of 2.5% which gives over 70% ion heating. Such a low He^3 level has a negligible impact on the reactivity. In fact, the reactivity is higher than in the $2\omega_{CT}$ case since a 50:50 D:T mixture can be used. A further advantage is that the ratio of ion damping to direct electron damping, by transit time magnetic pumping and Landau damping, is insensitive to $k_\parallel$ which gives scope to choose $k_\parallel$ for optimum antenna loading. This is the most promising ICRH scheme for ITER during the initial heating phase and, if the He^3 density is allowed

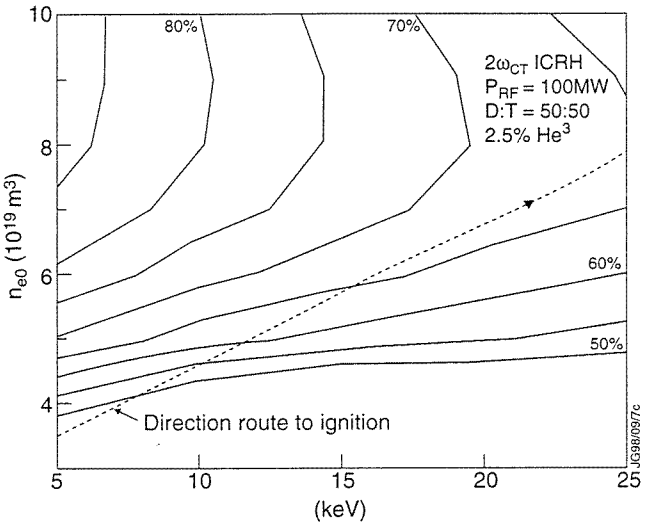

Figure 10. Contours of constant ion heating fraction for 50 MW of He^3 minority ICRH in ITER. The minority concentration is 2.5%.

to decrease, will convert automatically to the $2\omega_{CT}$ scheme as the plasma ion pressure increases.

3.2. Hydrogen minority heating

An example of hydrogen minority heating in an almost pure tritium plasma (D:T = 8:92), which has the strongest single-pass damping of all minority scenarios, is shown in figure 11. The plasma current for this discharge (41759) was 3.2 MA and the toroidal field was 3.4 T. The hydrogen concentration was 4% and its fundamental resonance was in the plasma centre; the RF frequency was 52 MHz. A power level of 8 MW produced a central electron temperature of 12 keV at a density of 2.8×10^{19} m^{-3}. A similar temperature was achieved with the same power using He^3 minority in discharge 42754 which is also shown in figure 11. For the H-minority discharge there was no measurement of the central ion temperature since the diagnostic neutral beams were unavailable. However, a value of 7.5 keV can be deduced from the neutron emissivity under the assumption that the T_i profile is the same as in the He^3 case. Thus, the hydrogen minority predominantly heats the electrons unlike the He^3 minority which gives equal power to electrons and ions to produce $T_{i0} = 12.5$ keV and $T_{e0} = 11$ keV. The confinement enhancement factor H97 = 0.85 for the (H)DT case is also lower than the (He^3)DT case probably due to orbit broadening of the heating profile in the former case. Similar efficient heating with H minority has been observed in TFTR.

In JET, H-minority ICRH played a vital role in the high-performance, hot-ion H-mode discharges that led to a record fusion power of 16 MW [22]. The ICRH, at a power level of 3 MW, was used to control the sawteeth in order to maximize the fusion output. An example is shown in figure 12 where two 3.8 MA discharges, one with and one without RF, are compared. The plasma with 3 MW of central H-minority heating had a minor sawtooth at 12.3 s compared with a more serious collapse at 12.7 s in the beam-only case. The sawtooth control by the ICRF allowed a superior fusion output of 13 MW with 2 MW less NBI power.

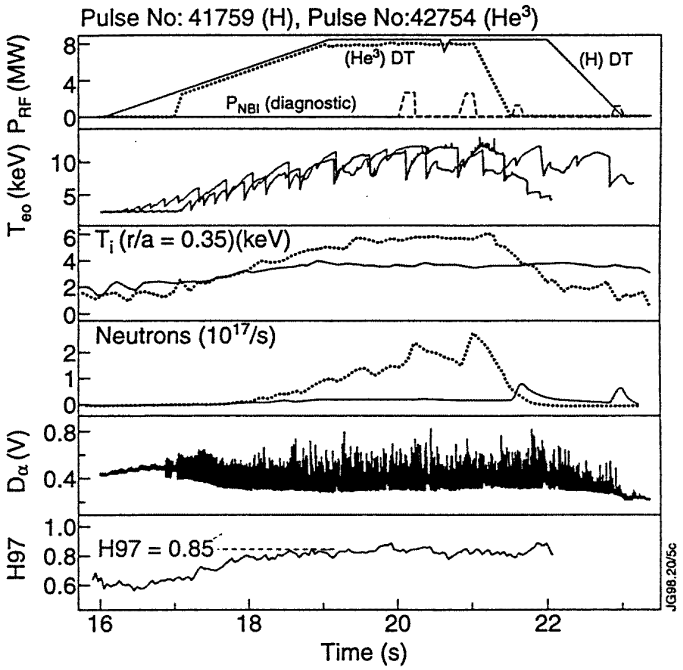

Figure 11. Hydrogen minority heating in a JET plasma with D:T = 8:92 giving a central electron temperature of 12 keV and an ion temperature of 7.5 keV.

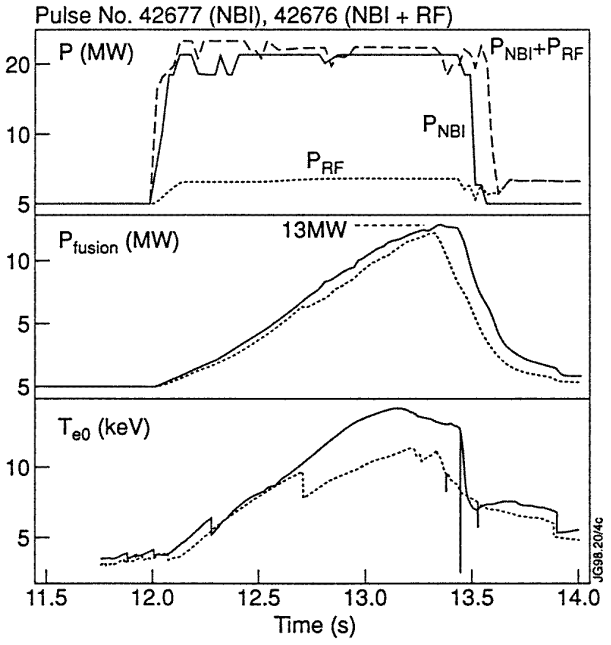

Figure 12. Sawtooth control with H-minority ICRH in a 3.8 MA hot ion H-mode which produced 13 MW of fusion power. A comparison NBI-only discharge suffered a large sawtooth crash at $t = 12.7$ s which diminished the performance.

3.3. Tritium minority in deuterium plasmas

During the programme to remove tritium from the JET vessel walls the heavy minority scheme of tritium minority in a deuterium plasma was investigated. In such schemes, cold plasma theory predicts that a fast wave cut-off occurs between the antenna and the minority resonance.

However, as the ion temperature becomes sufficiently high to allow the Doppler-broadened resonance to overlap the cut-off, the fast wave can be absorbed by cyclotron damping without tunnelling through the cut-off region. For a tritium minority of 5% in the 3.7 MA, 3.8 T discharges used in the JET experiment, the critical ion temperature was calculated to be about 2 keV. This value is close to that achieved experimentally; $T_i \sim 2.2$ keV at the resonance position. The resonance was 0.36 m on the high-field side of the magnetic axis which was the closest position to the plasma centre since the lowest ICRF frequency is 23 MHz on JET and the highest toroidal field is 3.8 T. The RF plant had never previously been used at this frequency and the loading was about 0.7 Ω requiring high voltage on the antennas and feed lines to achieve significant power. As a result, an unsteady 1.7 MW was delivered to the plasma from two antennas as shown in figure 13. At $t = 15$ s deuterium diagnostic beams were injected to measure the ion temperature profile. The central value was $T_{i0} = 3$ keV and the value at $r/a = 0.37$ was 2.0 keV in good agreement with the value given by the x-ray crystal spectrometer. The plasma density was 3.5×10^{19} m^{-3}. With the measured T_i profile the thermal D–T reaction rate is calculated to be 8×10^{14} s^{-1} which is 5% of the observed rate (1.5×10^{16} s^{-1}) just before the beam injection. Thus the fusion power is almost entirely generated by suprathermal reactions between accelerated tritons and the deuterium majority ions.

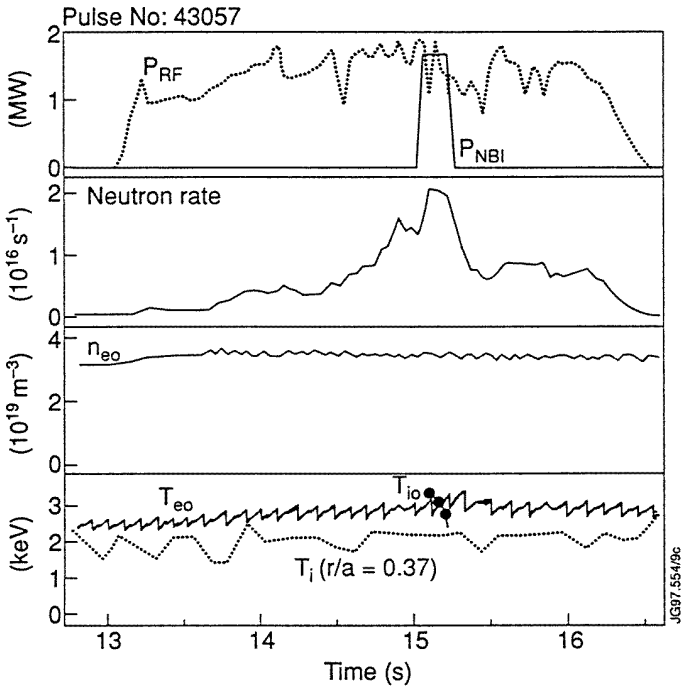

Figure 13. Suprathermal neutron production with (T)D ICRH.

The radial profile of the neutron emission obtained by tomographic reconstruction of the neutron camera data at $t = 14.9$ s is shown in figure 14. The emission is from an annulus of about 0.3 m radius with the maximum intensity corresponding to the calculated position of peak power absorption which is close to the location of the ion–ion hybrid layer. The reaction rate increases rapidly as the ICRF power increases as shown in figure 15. Preliminary calculations with a Stix model [23] for the fast triton distribution give a reasonably good representation of this behaviour which can only be reproduced if the tritons absorb at least 50% of the RF power. The formation of energetic triton tails have also been observed in TFTR with minority concentration of about 20% [24].

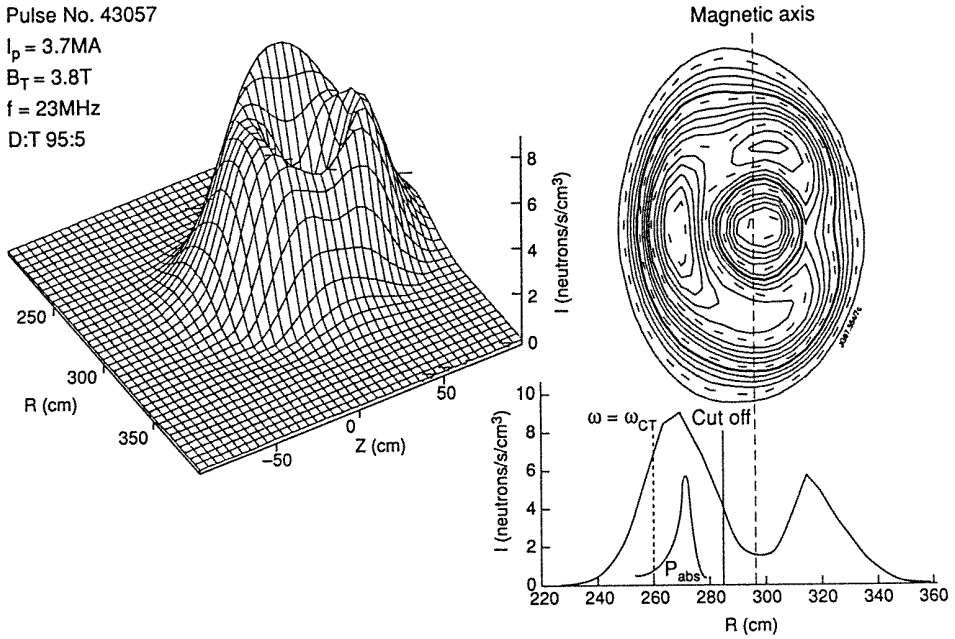

Figure 14. Tomographic reconstruction of the neutron camera data showing the neutron profile to be annular in form with a maximum yield close to the radius of the maximum power absorption. Note the position of the cut-off which lies between the low-field side antenna and the ω_{CT} resonance.

In the context of ITER, tritium minority heating is an excellent scheme for a preliminary tritium experiment with up to 10% tritium and the hydrogen minority scheme would provide efficient heating for deuterium plasmas in a pre D–T phase. However, the frequencies required at full field (5.8 T) for both hydrogen and tritium minorities, 87 MHz and 29 MHz respectively, are outside the range, 40–70 MHz, of the present design.

4. D–T mode conversion experiments in TFTR

These experiments were carried out in high-performance supershots with central ion temperatures in the region of 30 keV [2]. The toroidal magnetic field was 5.1 T which together with a frequency of 30 MHz and a D:T ratio of about 50:50 placed the mode conversion layer close to the plasma centre. A key feature in these experiments was the replacement of Li^7 by Li^6 for wall conditioning. In preliminary experiments during 1996,

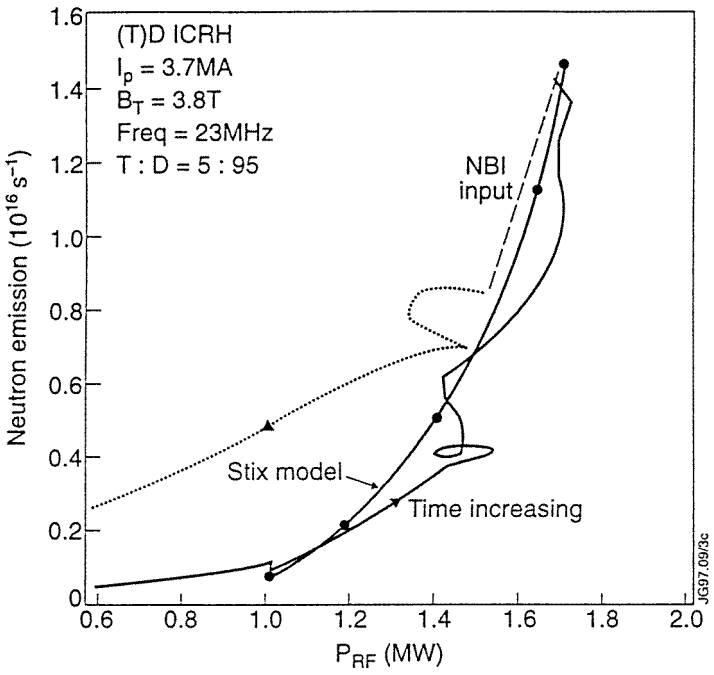

Figure 15. Suprathermal neutron emission as a function of ICRF power for the tritium minority scheme. The dotted curve is a Stix model calculation.

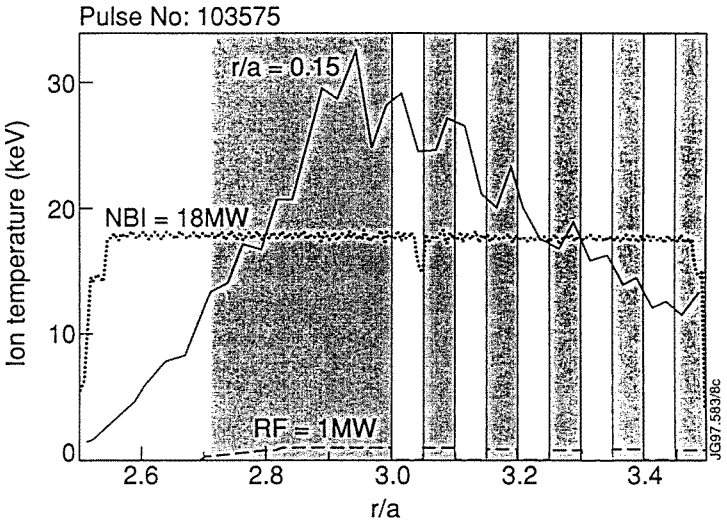

Figure 16. Ion temperature response to 1 MW of modulated mode conversion heating in TFTR.

0.7% Li^7 was found to absorb a substantial fraction of the RF power at its fundamental resonance which lies between the fundamental deuterium and tritium resonances and is close to the mode conversion layer. The addition of 1 MW of ICRH power to a discharge with 18 MW of NBI produced an increase of about 4 keV in the central ion temperature as shown

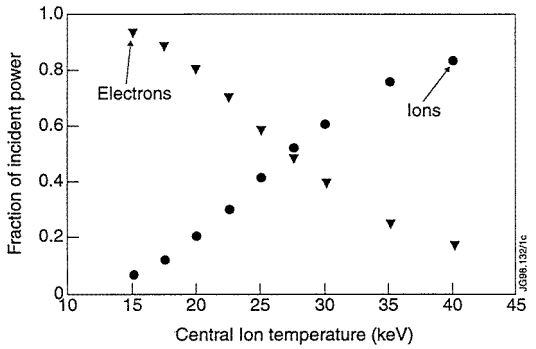

Figure 17. Strong ion heating by moded converted IBW is predicted by FELICE code at high T_i.

in figure 16. The temperature increase is readily observed as a modulation in synchronism with the RF power modulation. Note that the T_{i0} modulation decreases as the steady value of T_{i0} decreases. These results imply that at high ion temperatures in excess of 20 keV the IBW produced by the mode conversion is absorbed primarily by cyclotron damping. As T_i is reduced below 20 keV, electron damping of the IBW becomes the predominant absorption mechanism. This interpretation is confirmed by calculations with the FELICE code [2, 25] which predicts strong ion heating for sufficiently hot plasmas as shown in figure 17. For application to ITER this scheme requires the fast wave to be launched within the spectral range, 10 $m^{-1} < k_{\|} < 15$ m^{-1} and a frequency of 36 MHz which is almost inside the design range.

5. Summary and conclusions

The ion cyclotron heating experiments in D–T plasmas in JET and TFTR have established second-harmonic tritium and several minority scenarios as heating methods for ITER. Deuterium minority heating has produced the highest steady-state fusion Q-value of any heating system. ICRH is the only system which will produce predominantly central bulk ion heating on the ITER route to ignition, as has been demonstrated with the D and He^3 minority schemes on JET and with the second-harmonic tritium and mode conversion schemes on TFTR. The results for both neutron production and bulk ion heating are well reproduced by theoretical calculations using the TRANSP and PISCES codes for TFTR and the PION code for JET. H-modes have been produced in JET with confinement enhancement values above that required for ignition on ITER. The low-amplitude, high-frequency ELMs transport a fractional energy content of less than 1.5% which is close to the limit needed by ITER. Both the JET and TFTR experiments have raised the tritium minority heating scheme from the level of a scientific curiosity to a viable heating method.

References

[1] Bosia G, Elio R, Makowski M, Tonon G, ITER Joint Central Team, ITER Home Teams 1996 *Proc. 16th IAEA Conf. on Fusion Energy (Montreal, 1996)* vol 2 (Vienna: IAEA) p 917
[2] Majeski R *et al* 1997 *Proc. 12th Top. Conf. on Radio Frequency Power in Plasmas (Savannah, GA, 1997)* ed P R Ryan and T Intrator (New York: American Institute of Physics) p 73
[3] Wilson J R *et al* 1995 *Phys. Rev. Lett.* **75** 842
[4] Phillips C K *et al* 1995 *Phys. Plasmas* **2** 2427

[5] Majeski R *et al* 1995 *Proc. 22nd EPS Conf. on Controlled Fusion and Plasma Physics (Bournemouth, UK, 1995)* vol III, ed B E Keen, P E Stott and J Winter (Geneva: European Physical Society) p 365
[6] Wilson J R *et al* 1995 *Proc. 11th Top. Conf. on Radio Frequency Power in Plasmas (Palm Springs, CA, 1995)* ed R Prater and V S Chan (New York: American Institute of Physics) p 3
[7] Taylor G *et al* 1995 *Proc. 11th Top. Conf. on Radio Frequency Power in Plasmas (Palm Springs, CA, 1995)* ed R Prater and V S Chan (New York: American Institute of Physics) p 31
[8] Rogers J H *et al* 1997 *Proc. 12th Top. Conf. on Radio Frequency Power in Plasmas (Savannah, GA, 1997)* ed P R Ryan and T Intrator (New York: American Institute of Physics) p 13
[9] Hosea J C *et al* 1997 *Proc. 12th Top. Conf. on Radio Frequency Power in Plasmas (Savannah, GA, 1997)* ed P R Ryan and T Intrator (New York: American Institute of Physics) p 77
[10] Start D F H *et al* 1998 *Phys. Rev. Lett.* **80** 4681
[11] Jacquinot J *et al* 1985 *Plasma Phys. Control. Fusion* **27** 1379
[12] Korotkov A A, Gondhalekar A and Stuart A J 1993 *Nucl. Fusion* **33** 1037
[13] ITER Confinement Database and Modelling Working Group, presented by J G Cordey *Plasma Phys. Control. Fusion* **39** B115
[14] Eriksson L-G *et al*, this conference
[15] V P Bhatnagar *et al*, this conference
[16] Fasoli A *et al* 1997 *Plasma Phys. Control. Fusion* **39** B293
[17] Eriksson L-G, Hellsten T and Willen U 1993 *Nucl. Fusion* **33** 1037
[18] ITER Detailed Design Review 1996 *ITER Physics Basis and Performance Assessment* September
[19] Gormezano C, and references quoted therein, this conference
[20] Stix T H 1972 *Plasma Phys.* **14** 367
[21] Kukushkin A *et al* 1996 *Proc. 16th IAEA Conf. on Fusion Energy (Montreal, 1996)* vol 2 (Vienna: IAEA) p 987
[22] The JET Team, presented by Gibson A *Phys. Plasmas* **5** 1839
[23] Stix T H 1975 *Nucl. Fusion* **15** 737
[24] Phillips C K and Majeski R 1998 Private communication
[25] Brambilla M 1988 *Nucl. Fusion* **28** 549

Appendix

The JET Team. JET Joint Undertaking, Abingdon, Oxon OX14 3EA, UK

J M Adams[1], P Ageladarakis, B Alper, H Altmann, V Amasov[3], S Arshad, P Andrew, Y Andrew[12], D Bailey, N Bainbridge, B Balet, Y Baranov[8], P Barker, R Barnsley[2], M Baronian, D V Bartlett, A C Bell, L Bertalot[10], E Bertolini, V Bhatnagar, A J Bickley, H Bindslev, K Blackler, D Bond, T Bonicelli, D Borba[19], M Brandon, P Breger, H Brelen, P Brennan, W J Brewerton, M L Browne, T Budd, R Budny[14], A Burt, T Businaro, M Buzio, C Caldwell-Nicholls, D Campling, P Card, C D Challis, A V Chankin, D Chiron, J Christiansen, P Chuilon, D Ciric, R Claesen, H E Clarke, S Clement, J P Coad, I Coffey[7], S Conroy[16], G Conway[17], S Cooper, J G Cordey, G Corrigan, G Cottrell, M Cox[7], S J Cox, R Cusack, N Davies, S J Davies, J J Davis, M de Benedetti, H de Esch, J de Haas, E Deksnis, N Deliyanakis, A Dines, S L Dmitrenko, J Dobbing, N Dolgetta, S E Dorling, P G Doyle, H Duquenoy, A M Edwards[7], A W Edwards, J Egedal, J Ehrenberg, A Ekedahl[11], T Elevant[11], J Ellis, M Endler[13], S K Erents[7], G Ericsson[16], B Esposito[10], L G Eriksson, H Falter, J W Farthing, M Fichtmüller, G Fishpool, K Fullard, M Gadeberg, L Galbiati, A Gibson, R D Gill, D Godden, A Gondhalekar, D Goodall[7], C Gormezano, C Gowers, M Groth[18], K Guenther, H Guo, A Haigh, B Haist[4], C J Hancock, P J Harbour, N C Hawkes[7], N P Hawkes[1], J L Hemmerich, T Hender[7], J Hoekzema, L Horton, A Howman, M Huart, T P Hughes, F Hurd, G Huysmans, C Ingesson[15], B Ingram, M Irving, J Jacquinot, H Jaeckel, J F Jaeger, O N Jarvis, M Johnson, E M Jones, T T C Jones, J-F Junger, F Junique, C Jupen, J Kallne[16], A Kaye, B E Keen, M Keilhacker, W Kerner, N G Kidd, S Knipe, R Konig, A Korotkov, A Krasilnikov[3], J G Krom, P Kupschus,

R Lässer, J R Last, L Lauro-Taroni, K Lawson[7], M Lennholm, J Lingertat, X Litaudon[21], T Loarer, P J Lomas, M Loughlin, C Lowry, A C Maas[15], B Macklin, C F Maggi, M Mantsinen[5], V Marchese, F Marcus, J Mart, D Martin, G Matthews, H McBryan, G McCracken, P A McCullen, A Meigs, R Middleton, P Miele, F Milani, J Mills, R Mohanti, R Monk, P Morgan, G Murphy, F Nave[19], G Newbert, P Nielsen, P Noll, W Obert, D O'Brien, M O'Mullane, E Oord, R Ostrom, S Papastergiou, V V Parail, R Parkinson, W Parsons, B Patel, A Paynter, A Perevezentsev, A Peacock, R J H Pearce, M A Pick, J Plancoulaine, O Pogutse, R Prentice, S Puppin, G Radford[9], R Reichle, V Riccardo, F Rimini, F Rochard[21], A Rolfe, A L Roquemore[14], R T Ross, A Rossi, G Sadler, G Saibene, A Santaguistina, R Sartori, R Saunders, P Schild, M Schmid, V Schmidt, B Schokker[15], B Schunke, S M Scott, S Sharapov, A Sibley, M Simon, R Simonini, A C C Sips, P Smeulders, P Smith, R Smith, F Söldner, J Spence, E Springman, R Stagg, M Stamp, P Stangeby[20], D F Start, D Stork, P E Stott, J D Strachan[14], P Stubberfield, D Summers, L Svensson, P Svensson, A Tabasso[12], M Tabellini, J Tait, A Tanga, A Taroni, C Terella, P R Thomas, K Thomsen, E Traneus[16], B Tubbing, P Twyman, A Vadgama, P van Belle, G C Vlases, M von Hellermann, T Wade, R Walton, D Ward, M L Watkins, N Watkins[1], M J Watson, M Wheatley, D Wilson, T Winkel, D Young, I D Young, Q Yu[6], K-D Zastrow and W Zwingmann.

Permanent addresses

[1] UKAEA, Harwell, Didcot, Oxon, UK.
[2] University of Leicester, Leicester, UK.
[3] TRINITI, Troitsk, Moscow, Russia.
[4] KFA, Jülich, Germany.
[5] Helsinki University of Technology, Espoo, Finland.
[6] Institute of Plasma Physics, Hefei, People's Republic of China.
[7] UKAEA Culham Laboratory, Abingdon, Oxon, UK.
[8] A F Ioffe Institute, St Petersburg, Russia.
[9] Institute of Theoretical Physics, University of Oxford, UK.
[10] ENEA, CRE Frascati, Roma, Italy.
[11] Royal Institute of Technology, Stockholm, Sweden.
[12] Imperial College, University of London, UK.
[13] Max Planck Institut für Plasmaphysik, Garching, Germany.
[14] Princeton Plasma Physics Laboratory, Princeton, USA.
[15] FOM Instituut voor Plasmafysica, Nieuwegein, The Netherlands.
[16] Dept. of Neutron Research, Uppsala University, Sweden.
[17] University of Saskatchewan, Saskatoon, Canada.
[18] University of Manchester Institute of Science and Technology, Manchester, UK.
[19] IST, Centro de Fuseo Nuclear, Lisbon, Portugal.
[20] Institute for Aerospace Studies, University of Toronto, Canada.
[21] CEA, Cadarache, France.

The TFTR Team. Plasma Physics Laboratory, Princeton University, Princeton, New Jersey, United States of America

K M McGuire, C W Barnes[1], S H Batha[2], M A Beer, M G Bell, R E Bell, A Belov[3], H L Berk[4], S Bernabei, M Bitter, B N Breizman[4], N L Bretz, R V Budny, C E Bush[5], J D Callen[6], S Cauffman, C S Chang[7], Z Chang, C Z Cheng, G A Cottrell[8], D S Darrow,

R O Dendy[9], W Dorland[4], H Duong[10], P C Efthimion, D Ernst[11], H Evenson[6], N J Fisch, R Fisher[10], R J Fonck[6], C B Forest[10], E D Fredrickson, G Y Fu, H P Furth, V Ya Goloborod'ko[12], N N Gorelenkov[3], B Grek, L R Grisham, G W Hammett, G R Hanson[5], R J Hawryluk, W W Heidbrink[13], H W Herrmann, M Herrmann[5], K W Hill, J Hogan[5], B Hooper[14], J C Hosea, W A Houlberg[5], M Hughes[15], R A Hulse, D L Jassby, F C Jobes, D W Johnson, R Kaita, S M Kaye, J Kesner[11], J S Kim[7], M Kissick[6], A V Krasilnikov[3], H W Kugel, A Kumar[16], N T Lam[7], P LaMarche, B LeBlanc, F M Levinton[2], C Ludescher, J Machuzak[11], R Majeski, J Manickam, D K Mansfield, M E Mauel[17], E Mazzucato, J McChesney[11], D C McCune, G McKee[6], D M Meade, S S Medley, R Mika, D R Mikkelsen, S V Mirnov[3], D Mueller, Y Nagayama[18], G A Navratil[17], R Nazikian, M Okabayashi, D K Owens, H K Park, W Park, P Parks[10], S F Paul, M P Petrov[19], C K Phillips, M Phillips[15], P Phillips[4], A T Ramsey, M H Redi, G Rewoldt, S Reznik[12], J H Rogers, A L Roquemore, E Ruskov[13], S A Sabbagh[17], M Sasao[18], G Schilling, J Schivell, G L Schmidt, S D Scott, I B Senenov[3], T Senko, S Sesnic, C H Skinner, T Stevenson, W Stodiek, J D Strachan, E J Strait[10], B C Stratton, E J Synakowski, H Takahashi, W M Tang, G Taylor, J L Terry[11], M E Thompson, S Von Goeler, A Von Halle, R T Walters, S Wang[20], R B White, R M Wieland, M Williams, J R Wilson, K L Wong, G A Wurden[1], M Yamada, V Yavorski[12], K M Young, L E Zakharov, M C Zarnstorff and S J Zweben.

Permanent addresses

[1] Los Alamos National Laboratory, Los Alamos, New Mexico, USA.
[2] Fusion Physics and Technology, Torrance, California, USA.
[3] Troitsk Institute of Innovative and Thermonuclear Research, Moscow, Russian Federation.
[4] Institute for Fusion Studies, University of Texas, Austin, Texas, USA.
[5] Oak Ridge National Laboratory, Oak Ridge, Tennessee, USA.
[6] University of Wisconsin, Madison, Wisconsin, USA.
[7] Courant Institute, New York University, New York, NY, USA.
[8] JET Joint Undertaking, Abingdon, Oxfordshire, UK.
[9] Culham Laboratory, Abingdon, Oxfordshire, UK.
[10] General Atomics, San Diego, California, USA.
[11] Massachusetts Institute of Technology, Cambridge, Massachusetts, USA.
[12] Ukrainian Institute of Nuclear Research, Kiev, Ukraine.
[13] University of California, Irvine, California, USA.
[14] Lawrence Livermore National Laboratory, Livermore, California, USA.
[15] Northrop-Grumman Corporation, Princeton, New Jersey, USA.
[16] University of California, Los Angeles, California, USA.
[17] Columbia University, New York, NY, USA.
[18] National Institute for Fusion Science, Nagoya, Japan.
[19] A F Ioffe Physico-Technical Institute, St Petersburg, Russian Federation.
[20] Institute of Plasma Physics, Academia Sinica, Hefei, Anhui, People's Republic of China.